12-1-2023

Residual trapping of CO2, N2, and a CO2-N2 mixture in Indiana limestone using robust NMR coreflooding: Implications for CO2 geological storage

Amer Alanazi

Auby Baban
Edith Cowan University

Muhammad Ali

Alireza Keshavarz
Edith Cowan University

Stefan Iglauer
Edith Cowan University

See next page for additional authors

10.1016/j.fuel.2023.129221
Alanazi, A., Baban, A., Ali, M., Keshavarz, A., Iglauer, S., & Hoteit, H. (2023). Residual trapping of CO2, N2, and a CO2-N2 mixture in Indiana limestone using robust NMR coreflooding: Implications for CO2 geological storage. Fuel, 353, article 129221. https://doi.org/10.1016/j.fuel.2023.129221

Fuel 353 (2023) 129221

Contents lists available at ScienceDirect

Fuel

journal homepage: www.elsevier.com/locate/fuel

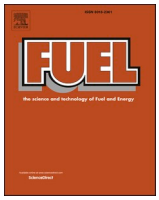

Full Length Article

Residual trapping of CO_2, N_2, and a CO_2-N_2 mixture in Indiana limestone using robust NMR coreflooding: Implications for CO_2 geological storage

Amer Alanazi [a,*], Auby Baban [b,*], Muhammad Ali [a], Alireza Keshavarz [b], Stefan Iglauer [b], Hussein Hoteit [a]

[a] Physical Science & Engineering Division, King Abdullah University of Science and Technology, Thuwal 23955, Saudi Arabia
[b] School of Engineering, Edith Cowan University, 270 Joondalup Drive, Joondalup WA 6027, Australia

ARTICLE INFO

Keywords:
Carbon dioxide and nitrogen
Wettability and geological storage
Indiana limestone
Imbibition and drainage
Nuclear magnetic resonance

ABSTRACT

Carbon capture and sequestration (CCS) in geological formations is a prominent solution for reducing anthropogenic carbon emissions and mitigating climate change. The capillary trapping of CO_2 is a primary trapping mechanism governed by the pressure difference between the wetting and nonwetting phases in a porous rock, making the latter a key input parameter for dynamic simulation models. During the CCS operational process, however, the CO_2 is prone to contamination by impurities from various sources such as surfaces (e.g., pipelines and tanks) and the subsurface (e.g., existing natural gas). Such contamination can strongly influence the overall CO_2 wettability, storage capacity, and containment security. Hence, the present study uses the nuclear magnetic resonance (NMR) core flooding technique to investigate and compare the residual saturations of pure CO_2, pure N_2, and a 50:50 CO_2/N_2 mixture in an Indiana limestone. The longitudinal and transverse relaxation times (T_1 and T_2) are measured to examine the displacement process of the pore network, and the trapping mechanism is evaluated at the pore scale as a determinant of the field-scale flow behavior. The NMR T_1-T_2 and 2D maps are used to observe the fluid configurations in the pore network, and the T_1/T_2 ratios are used to evaluate the microscopic wettability of the limestone grains by the pore-space fluids following each drainage/imbibition process step. The results indicate substantial residual gas trapping in the rock for the CO_2-brine, N_2-brine, and CO_2/N_2-brine systems, corresponding to gas saturations of 25%, 27%, and 26%, respectively. In the CO_2-brine system, the intermolecular interplay between the CO_2-enriched brine and limestone grains results in a higher T_1/T_2 ratio and significantly reduces the hydrophilicity of the limestone. Furthermore, the NMR T_2 distribution reveals the occurrence of preferential water displacement into the large pores ($r > 1$ μm) and from the intermediate pores (0.03 μm $< r <$ 1 μm), whereas water remains immobile in the smaller pores ($r <$ 0.03 μm). The insignificant difference in residual trapping saturation between pure CO_2 and the CO_2-N_2 mixture indicates the potential to allow for impurities in the CO_2 phase in CCS without reducing the residual trapping capacity. Thus, the present work provides comprehensive information on the impact of gas injection on residual gas trapping in subsurface geological formations at the pore scale, thereby aiding in the development of CCS and other potential applications in enhanced oil recovery (EOR).

1. Introduction

The rapid increases in energy demand and anthropogenic carbon emissions impose global, governmental, environmental, and technological challenges [1–4]. As a result, decarbonization plans and strategies must be expedited to curb the observed carbon emissions [5]. Carbon geological sequestration (CGS) technology is highly regarded as part of the strict environmental regulations adopted by countries and governments to reduce carbon emissions and limit global warming [6,7]. In this approach, carbon dioxide (CO_2) is captured from high-emission sectors and injected into geological formations such as deep saline aquifers and depleted hydrocarbon reservoirs [8–11]. The primary trapping mechanisms for the sequestration of CO_2 in geological formations are stratigraphic (structural), capillary, solubility, and mineral trapping [12,13]. In structural trapping, the captured CO_2 is injected in its supercritical phase ($scCO_2$) so that it percolates upward

* Corresponding authors.
E-mail addresses: amer.alanazi@kaust.edu.sa (A. Alanazi), a.baban@ecu.edu.au (A. Baban).

https://doi.org/10.1016/j.fuel.2023.129221
Received 3 April 2023; Received in revised form 22 June 2023; Accepted 11 July 2023
Available online 19 July 2023

due to the buoyancy difference with respect to the formation fluids and is trapped under a caprock [14,15]. Meanwhile, in capillary trapping (also known as residual trapping), the CO_2 is trapped in the pore space as isolated bubbles at the trailing edge of the plume independently of the caprock, as it is naturally displaced by groundwater as the plume migrates upwards due to buoyancy forces [16]. In the larger pores, where CO_2 is the non-wetting phase, water preferentially fills the narrower areas of the pore space and traps the gas by snap-off [17]. In either case, the CO_2 wettability of the reservoir rock or the caprock significantly impacts the petro-physical properties (capillary pressure, relative permeability, saturation, and pore-size distribution) of the system [18], and is crucial for predicting the CO_2 geo-storage capacity and containment security. The CO_2 wettability controls the distributions and flow characteristics of fluids (brine and CO_2) in the pore network of the formation rock, which strongly affects the residual trapping mechanism [19]. For instance, oil and gas reservoirs often range from oil-wet to weakly water-wet [20,21] due to the attraction between the rock surface and the polar water molecules, which is detrimental to their CO_2 trapping and storage capacities [22–26].

However, despite the continuing advancements in CO_2 geo-storage, there remain significant uncertainties regarding the fundamental aspects of multiphase flow mechanics and the prediction of subsurface trapping and CO_2 migration. For instance, while numerous studies have used experimental techniques such as core flooding [27,28], microfluidics [29–32], micro-CT scan and X-ray [33–35], and contact angle measurements [5,36,37] to investigate the injection of pure $scCO_2$, the fundamental impact of impurities on CO_2 residual trapping and containment security remain largely uncertain [38–41]. Such impurities alter the thermo-physical properties of the pure $scCO_2$ and directly influence the hydrodynamic, solubility, and capillary CO_2 trapping mechanisms [38,39,42–45]. Meanwhile, field CGS projects are expensive and entail conveyance, underground injection, and CO_2 capture from industrial operations. The capture and separation of CO_2 from common contaminants such as nitrogen (N_2), oxygen (O_2), argon (Ar), and sulfate groups (SO_x) remain costly, even though CGS projects are frequently combined with enhanced oil recovery (EOR) to offset the cost [2,46,47]. Consequently, it is more economical to tolerate some impurities in the CO_2 during the injection process, even though such impurities may reduce the CO_2 geo-storage capacity and containment efficiency [48]. Moreover, the co-storage of CO_2 with pollutants removed from other sources is presently being investigated for potential environmental and economic applications [49–54].

In the present work, nuclear magnetic resonance (NMR) combined with core flooding is used to study three gases (namely, CO_2, N_2, and a 50:50 CO_2-N_2 mixture) within brine-saturated core plugs to examine the effect of impurity on the residual trapping of CO_2 [55]. The longitudinal and transverse relaxation times (T_1 and T_2) are measured, and the in-situ NMR T_1-T_2 2D images are obtained for an initial brine-saturated plug and after multiple drainage/imbibition cyclic processes to determine the initial and residual CO_2 saturations ($S_{CO2,i}$ and $S_{CO2,r}$, respectively). The present work aims to provide an improved understanding of the $scCO_2$ flow processes through water-saturated porous rock in CO_2-brine-rock systems. The results provide insights into the relative performances of CGS with pure CO_2, pure N_2, and an impure CO_2 proxy (50:50 CO_2-N_2). Furthermore, the work represents the first comprehensive dataset showing that the use of CO_2 in the presence of a contaminat may be a cost-effective technology.

2. Experimental procedures and materials

2.1. Rock sample, fluids, and testing conditions

Indiana limestone has been used in laboratory experiments as a representative reference for carbonate reservoirs. It is quarried from the Salem Formation in Indiana, USA, which was formed during the Mississippian age [56]. It mainly comprises calcite-cemented grainstone of fossil fragments and oolites [57,58]. In the present work, cylindrical core Indiana limestone samples with lengths of 5 cm and diameters of 3.7 cm were used in all experiments. The morphology of the Indiana limestone was examined by scanning electron microscopy (SEM; Quattro SEM instrument), and its chemical composition was determined via X-ray diffraction (XRD; Bruker-AXS D8 Advance Diffractometer). Thus, the Indiana limestone is a heterogeneous rock type with a broad pore size distribution including intergranular and intragranular micropores (Fig. 1) and consists of 88 wt% calcite, 11 wt% magnesium, and 1 wt% quartz (Fig. 2). Moreover, the sample has a porosity of 17.4 ± 0.5% and a permeability of 50 mD (as measured using a CoreLab UltraPoroPerm-910 instrument).

Ultra-pure (99.999%) CO_2 and N_2 (BOC Industrial Gases, WA) were used as the nonaqueous fluid phases in the core-flooding experiments. Pure N_2 was used as a benchmark nonwetting phase for comparison with the results obtained using CO_2, and was selected because of its well-constrained thermophysical properties, its closer viscosity to that of CO_2 than that of liquid hydrocarbons, and the lack of any need for a cleaning step between each repeat measurement [59,60]. Brine (2 wt% NaCl + 1 wt% KCl in deionized water) was used as the aqueous phase, while N_2, $scCO_2$, and a 50:50 mixture of CO_2 and N_2 were used as the nonaqueous fluid phases. To simulate reservoir conditions, high pressure and high temperature (HPHT) values of 8 MPa and 333 K were applied so that the CO_2 was in its supercritical state with a higher density, viscosity, and enhanced wettability [61–63]. Notably, the injection of CO_2 in its supercritical state is commonly used to increase the mass of stored CO_2 [64–66].

2.2. Core-flooding experimental setup and procedure

The limestone core sample was first vacuum-dried at 333 K for 24 h, then wrapped in a polytetrafluoroethylene (PTFE) heat-shrink rubber sleeve with the ends left open for the injection and desaturation of fluids. The sleeve was sealed in such a way as to overlap with the top and bottom platens of the core holder to adequately separate the core fluids from the confining fluid, and to prevent any leakage of the confining fluid (Fluorinert^{TM} FC-40) into the sample. The latter was used to apply a confining pressure, and each fluid was controlled by an individual ISCO pump. Fluorinert^{TM} FC-40 was selected as a non-hydrogenated fluid that does not interfere with the NMR signal and has superior heat transmission characteristics. The sealed plugs were mounted in the NMR apparatus, as depicted in Fig. 3. Before starting the core flooding experiment, the fluid lines and core were flushed with CO_2 to remove air from the system while applying a confining pressure of 1 MPa. The core was then pressurized to 8 MPa with a confining pressure of 13 MPa, and the system was isothermally heated to 333 K. The core flooding experiment was started by injecting 10 pore volumes (PV) of 'dead' (i.e., gas-free) brine at a low flow rate of 0.5 mL/min to allow the flow process to be dominated by the capillary force (capillary number (N_c) = 4.75×10^{-6}) [67]. After acquisition of the background NMR T_2 scans, the core was flooded at 0.5 mL/min with 10 PV of 'live' brine (i.e., brine that was thermodynamically equilibrated (saturated) with CO_2 at 8 MPa and 333 K [58]) until all of the dead brine was displaced. The displacement of the dead brine was confirmed by performing multiple T_2 scans that showed a constant T_2 value [18]. This step was necessary to ensure that no mass transfer effects interfered with the experiment [68]. Experiments were then performed with either $scCO_2$ and water, N_2 and water, or a CO_2-N_2 mixture as the fluid phase. The core-flooding commenced with the injection of the selected fluid (10 PV) at a constant flow rate of 0.5 mL min^{-1} (N_c = 9.5×10^{-7}, drainage) [18,55] into the fully live-brine saturated core at 8 MPa and 333 K to displace the local brine until steady-state conditions were reached (i.e., no more brine displacement and no variation in T_2 were observed). Throughout the experiments, the outlet pressure was maintained at 8 MPa by using an ISCO pump as a back-pressure source. Once the pressure drop had stabilized, the T_1-T_2 spectra and multiple NMR T_2 scans for the core at this initial gas

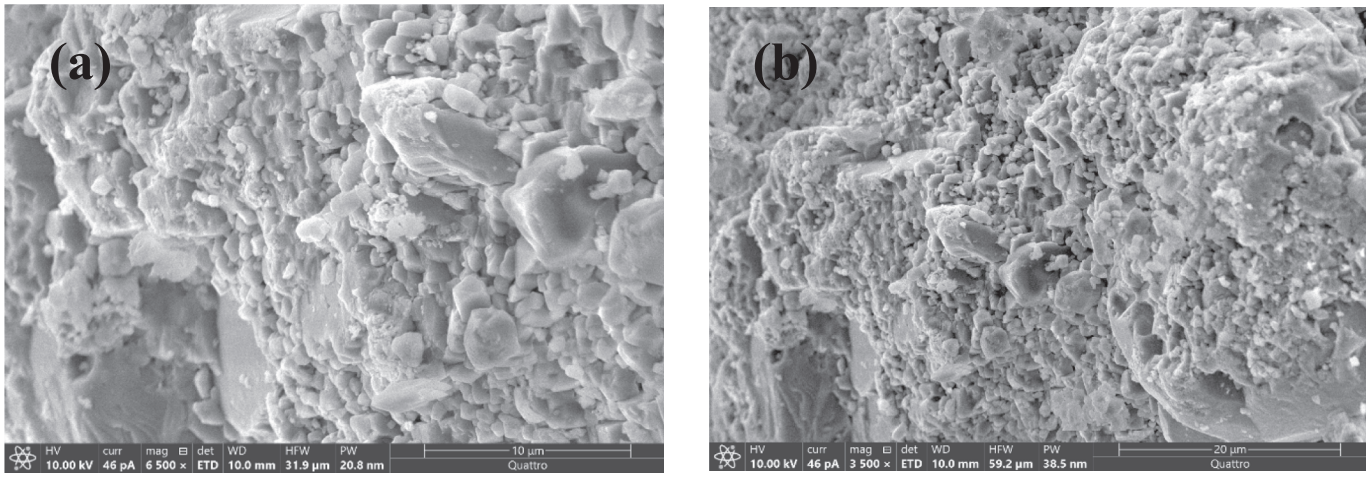

Fig. 1. SEM images of a thin section taken from the Indiana limestone core sample: (a) scale bar = 10 μm; (b) scale bar = 20 μm.

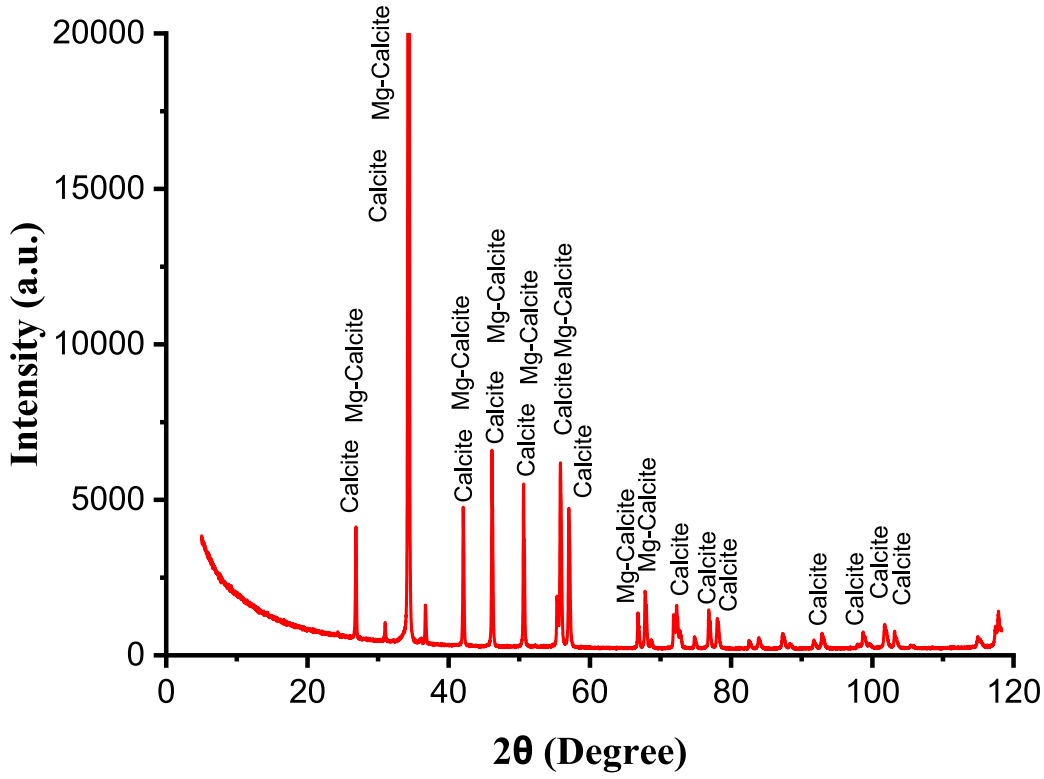

Fig. 2. The XRD pattern of the Indiana limestone core sample, indicating high contents of calcite and magnesium.

saturation (S_{gi}) were acquired. Subsequently, 10 PV of live brine was re-injected at 0.5 mL min^{-1} (i.e., $N_c = 4.75 \times 10^{-6}$) to mimic the replacement of the buoyant injected $scCO_2$ by brine (imbibition either by natural water influx or water injected by pumps). This represents the capillary trapping process in which residual CO_2 saturation (S_{gr}) is achieved.

2.3. NMR T_1-T_2 2D map and T_2 relaxation time measurements

In accordance with the literature, the fluid saturations, pore size distributions, and pore-fluid distributions were determined by measuring the longitudinal and transverse relaxation times (T_1 and T_2, respectively) [59,69,70] and obtaining the corresponding T_1/T_2 ratios from the 2D T_1-T_2 maps [18,72,73]; the latter were used to evaluate the surface affinity between the wetting phase and the rock (i.e., the microscopic wettability) [71,87]. The T_2 relaxation time distribution is primarily governed by surface relaxation processes, which depend on the interactions between the fluids in the pore space [74,75]. Hence, the surface relaxation rate ($1/T_{2,surf}$) of the pore fluid in the fast diffusion limit is given by Eq. (1) [76]:

$$\frac{1}{T_2} = \rho_2 \left(\frac{S}{V}\right)_{pore} \tag{1}$$

where ρ_2 is the effective surface relaxivity (SR), S is the interstitial surface area (μm^2), and V is the pore volume (PV; μm^3). The SR (ρ_2) relates the pore voids to T_2 and depends on the rock mineralogy; for Indiana limestone, $\rho_2 \approx 7$ $\mu m.s^{-1}$ [77]. The ratio S/V can be rewritten as a function of the dimensionless shape factor (C_s) and pore radius (r) in

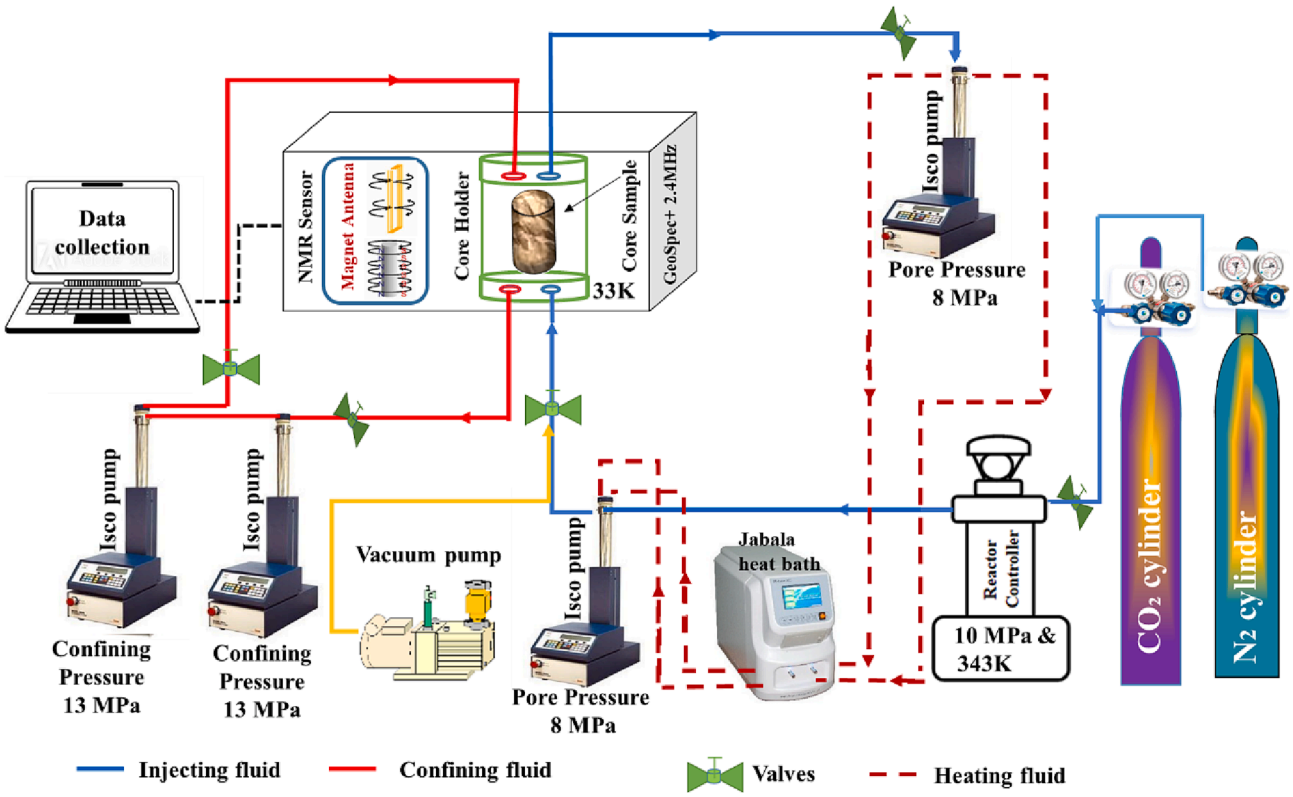

Fig. 3. A schematic diagram of the of NMR core flooding apparatus.

μm. Assuming that the pores are spherical ($C_s = 3$) and that $T_{2,surf} \ll T_{2,bulk}$ [78], the pore size distribution can be approximated using Eq. (2):

$$r = C_s \rho_2 T_2 \quad (2)$$

3. Results and discussion

3.1. T_1-T_2 Mapping and fluid configuration

To quantify the CO_2 residual trapping capacities, the NMR 2D T_1-T_2 spectra and transverse relaxation times (T_2) of the hydrogen nuclei in the water-wet limestone core were measured under reservoir conditions (333 K and 8 MPa), and the results are presented in Tables 1 and 2, and Figs. 4 and 5. Thus, when fully saturated with water, the core exhibits an initial T_1/T_2 value of 1, thereby indicating that the rock is hydrophilic (strongly water-wet). It should be noted that single-phase low viscosity fluids (e.g., water) and light hydrocarbons have similar T_1 and T_2 relaxation times (i.e., $T_1/T_2 = 1$) because of their rapid correlation times (τ_c) at the Larmor frequency (Fig. 4**a**) [18,55,59,72,73,79]. Moreover, the T_1/T_2 ratio of the core sample remains unchanged after N_2 injection (Fig. 4**b**), but is considerably increased to $T_1/T_2 = 3$ after the introduction of CO_2 (Fig. 4**c**). This suggests a significant decrease in the hydrophilicity and, hence, the physicochemical surface affinity of the rock grains to water [26,80,81]. This, in turn, is due to the much higher density of CO_2 (191.95 kg.m^{-3}) compared to that of N_2 (79.81 kg.m^{-3}) under the selected reservoir conditions [82], and is consistent with earlier contact angle studies showing that the de-wetting of the rock surface is caused by an increase in the pressure of CO_2 [83,84]. The results are also consistent with a previous study in which the contact angle of a water-wet carbonate rock surface was shown to increase significantly with the increase in CO_2 density[85].

Mechanistically, the water-wetness of the rock is significantly lowered via the interaction between the limestone rock grains and the excess protons (H^+) generated by the chemical reaction of the dissolved CO_2 in the formation brine to form carbonic acid (H_2CO_3), which partially dissociates into H^+ and negatively-charged ions such as HCO^{3-} and CO_3^{2-} [59,86]. When the $scCO_2$ advances in the pore space, it displaces the water from the large pores and confines it to forming thick wetted layers in the restricted narrow throats [66,88,89]. Thus, the dense macroscopic water layers that form and coat the grain surfaces due to the rock's strong affinity for the water phase occupy the smallest

Table 1
The NMR T_1/T_2 ratios of a water-wet Indiana limestone sample after the processes of dead brine saturation, N_2 injection, CO_2 injection, 50:50 CO_2-N_2 injection, and live brine injection (imbibition).

Process	Live brine	N_2 injection	CO_2 injection	CO_2-N_2 mixture (50–50%) injection	Live brine re-injection
T_1/T_2 for water-wet Indiana Limestone sample	1	1	3	2	1.8

Table 2
The measured saturations of CO_2, N_2, and 50:50 CO_2-N_2 at 8 MPa and 333 K during secondary drainage ($S_{nonwetting,i}$) and imbibition ($S_{nonwetting,r}$) as a function of injected pore volume (PV) for a water-wet Indiana limestone core plug.

Injected PV	CO_2 T_2 (*ms*)	$S_{CO2,i}$	N_2 T_2 (*ms*)	$S_{N2,i}$	50:50 CO_2-N_2 T_2(*ms*)	($S_{CO2\text{-}N2,i}$)
0.5	0.16	0.087	0.16	0.087	0.15	0.143
1	0.15	0.146	0.147	0.156	0.14	0.201
2	0.14	0.189	0.133	0.237	0.125	0.282
3	0.13	0.252	0.12	0.315	0.116	0.335
4	0.11	0.370	0.1	0.415	0.109	0.377
5	0.09	0.507	0.083	0.526	0.087	0.499
10	0.085	0.52	0.073	0.584	0.081	0.536

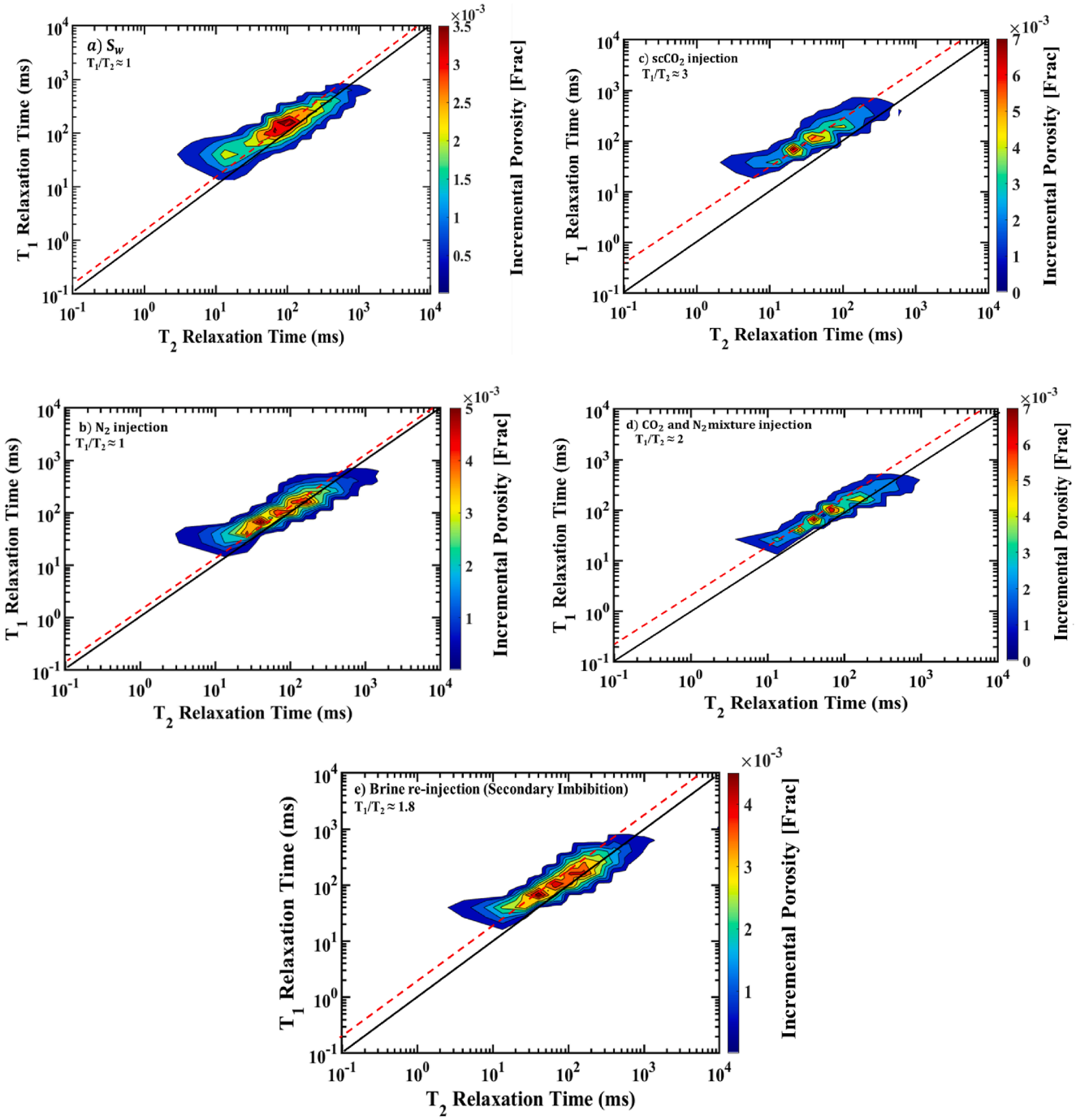

Fig. 4. The NMR T_1-T_2 maps of the water-wet Indiana limestone core at 8 MPa and 333 K: (a) in the initial fully brine-saturated state (Sw), (b) after N_2 injection, (c) after CO_2 injection, (d) after injection of the 50:50 CO_2-N_2 mixture, and (e) after the re-injection of brine for secondary imbibition. In each case, the black diagonal line represents $T_1 = T_2$.

pores of the Indiana limestone, while the nonwetting phase (CO_2) occupies the large pores [88,89]. However, the T_1/T_2 ratio does not return to its initial value of 1 after secondary imbibition (Tables 1 and 2, Fig. 4**e**), remaining at ~ 1.8 even after the injection of the 50:50 CO_2-N_2 mixture (Table 1), and the rock exhibits a decreased hydrophilicity (Fig. 4**d**).

3.2. The T_2 relaxation time and pore-scale fluid distributions

3.2.1. Gas coreflooding – Initial gas saturation (S_{gi})

The NMR T_2 time distributions during injection of the various gases (N_2, CO_2, and 50:50 CO_2-N_2) are compared in Fig. 5. Here, the solid lines represent the incremental porosity, while the dashed lines represent the cumulative porosity. Each plot exhibits a trimodal distribution after the introduction of the nonwetting phase. The first measurement represents the Indiana Limestone rock sample in its initial fully water-saturated state (Sw; black lines, Fig. 5**a–c**), and subsequent T_2 measurements were obtained for each pore volume (0.5, 1, 2, 3, 4, 5, and 10) of injected gas. These measurements are summarized in Table 2. Thus, the incremental T_2 (which is proportional to the cumulative T_2) decreases as the injected gas progresses further into the pore system until no more water displacement is observed (S_w = 0.085 *ms*) at 10 PV (green curves, Fig. 5**a–c**). Due to the different gas densities, the measured cumulative T_2 relaxation times for CO_2 are slightly lower than those for N_2.

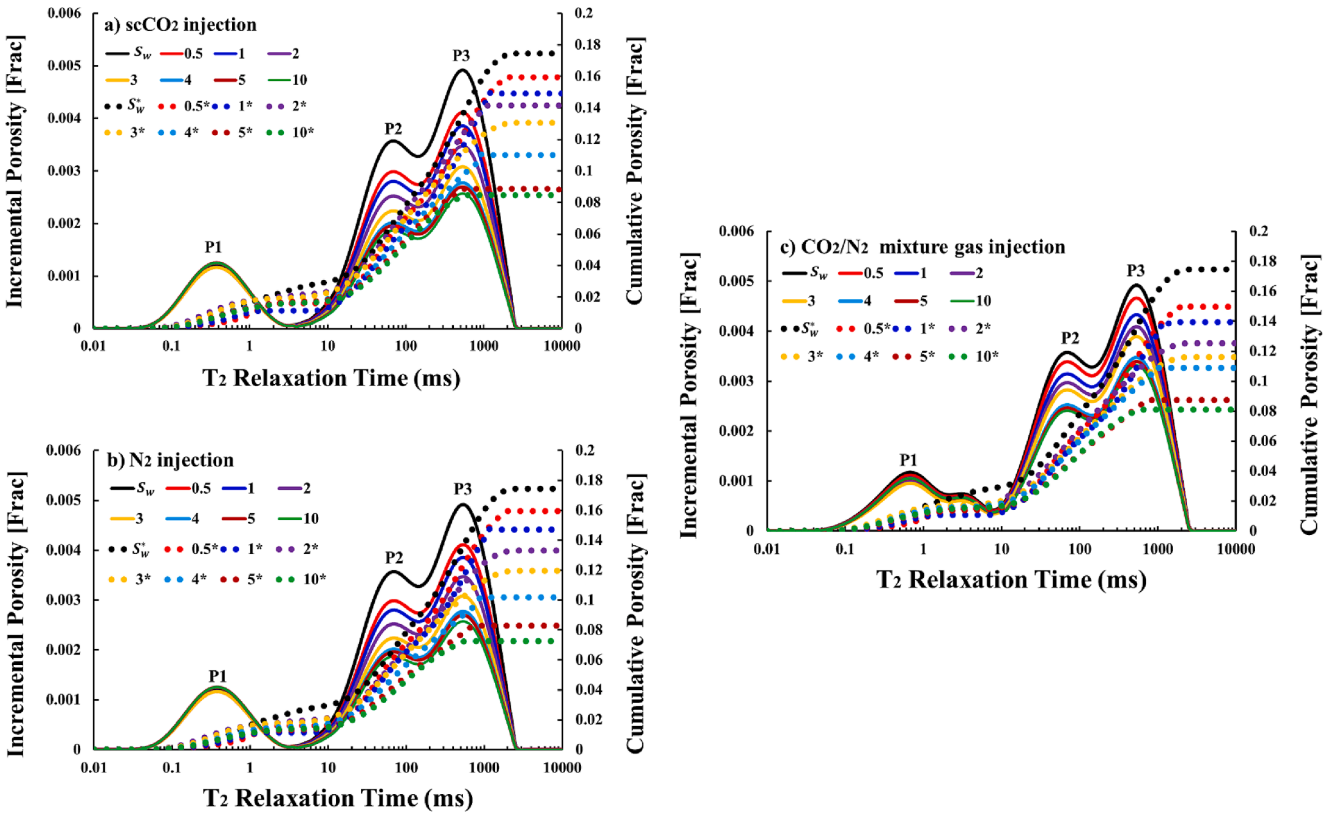

Fig. 5. The T_2 relaxation time profiles of the water-wet Indiana limestone core at 8 MPa and 333 K after coreflooding with various non-wetting gases: (a) $scCO_2$, (b) N_2, and (c) 50:50 CO_2-N_2. The asterisk (*) in the key represents the cumulative porosity, which is indicated by the dashed lines, while the solid lines represent the incremental porosity.

Moreover, as the contact angle is linearly related to the gas density [85], the higher density of CO_2 relative to that of N_2 means that the CO_2/brine/rock system has a larger contact angle (and, hence, a significantly lower hydrophilicity) than does the N_2/brine/rock system. Furthermore, although exposure to CO_2 renders the core sample less water-wet, the same initial gas saturation (S_{gi}) is measured for CO_2, N_2, and the CO_2-N_2 mixture. This is primarily because the dissolution of the limestone surface during live brine flooding decreases the water-wetness of the CO_2/brine/rock system due to changes in the microstructures (morphological connectivities) of the intermediate-sized pores (P2; 0.03 μm < r < 1 μm) and of the large pores (P3; 1 μm < r) [90–92]. Specifically, the thinner pore walls are dissolved by the acidic brine, which then flows down the newly-formed larger channels. Thus, the surface potential and polarity of the rock surface are reduced, resulting in a more electrically neutral surface with a correspondingly lower affinity for the polar H_2O molecule (i.e., a lower hydrophilicity) [26,59,80,93]. This, in turn, effectively reduces the bulk T_2 relaxation time of the brine. This is manifested by the reduction in T_2 (water saturation) for peaks P2 and P3 in Fig. 5**a–c** as the CO_2 displaces water predominately from the macro-pores and also from the mesopores [18,59,95,96]. By contrast, no variation is observed in the T_2 signals for the small pores (P1; r < 0.03 μm), thereby indicating that water remains in the smallest pores, which is characteristic of a hydrophilic system. This is predominantly due to the constrained geomechanical characteristics of the fluid in the small, tightly-packed pore network, which lead to minimal (or negligible) changes in the tensile and shear strength of the fine pore system and, hence, to a very low probability of bond-breaking or detachment of microparticles from the pore surface [94]. Finally, after the injection of 10 PV of CO_2, N_2, or 50:50 CO_2-N_2, the water content in the core has decreased to irreducible water saturation (S_{wirr}) values of 48%, 42%, and 46%, respectively (Fig. 5; Table 3), which is consistent with the literature [90,95,97]. Consequently, significant initial gas saturations ($S_{CO2,i}$ = 52%, $S_{N2,i}$ = 58%, and $S_{CO2\&N2,i}$ = 54%) were achieved, in good agreement with previous μ-CT studies on water-wet limestone [92,98] and similar studies on other water-wet systems [99–101].

Table 3
The gas saturations of the water-wet Indiana limestone core plug during secondary drainage and secondary imbibition as a function of injected pore volume at 8 MPa and 333 K.

Gas	Initial gas saturation after secondary drainage ($S_{g,i}$) (%)	Water saturation after secondary drainage (S_w) (%)	Residual gas saturation after secondary imbibition ($S_{g,r}$) (%)	Water saturation after secondary imbibition (S_w) (%)
CO_2	52	48	25	75
N_2	58	42	27	73
50:50 CO_2-N_2	54	46	26	74

3.2.2. *Pore-size distribution and capillary trapping*

The results in Fig. 6 and Table 4 indicate that after live brine injection (re-imbibition), water has invaded the pore space and displaced the nonwetting phase (CO_2, N_2, or 50:50 CO_2/N_2) to reoccupy the intermediate-sized pores (0.03 < r < 1 μm) and the large pores (r > 1 μm). With the re-injection of 10 PV of live brine, the water saturation is seen to increase gradually from 52%, 58%, and 54% for the CO_2/brine, N_2/brine, and 50:50 CO_2/N_2/brine system, respectively, before reimbibation, to 76%, 74%, and 75%, respectively, afterwards (Fig. 6**a–c**). However, as expected, brine re-injection does not remove all of the gas, but leaves a residual gas saturation ($S_{g,r}$) of 25% CO_2, 27 % N_2, and 26% 50:50 CO_2/N_2 (Table 3), which is predominately stored in the large and

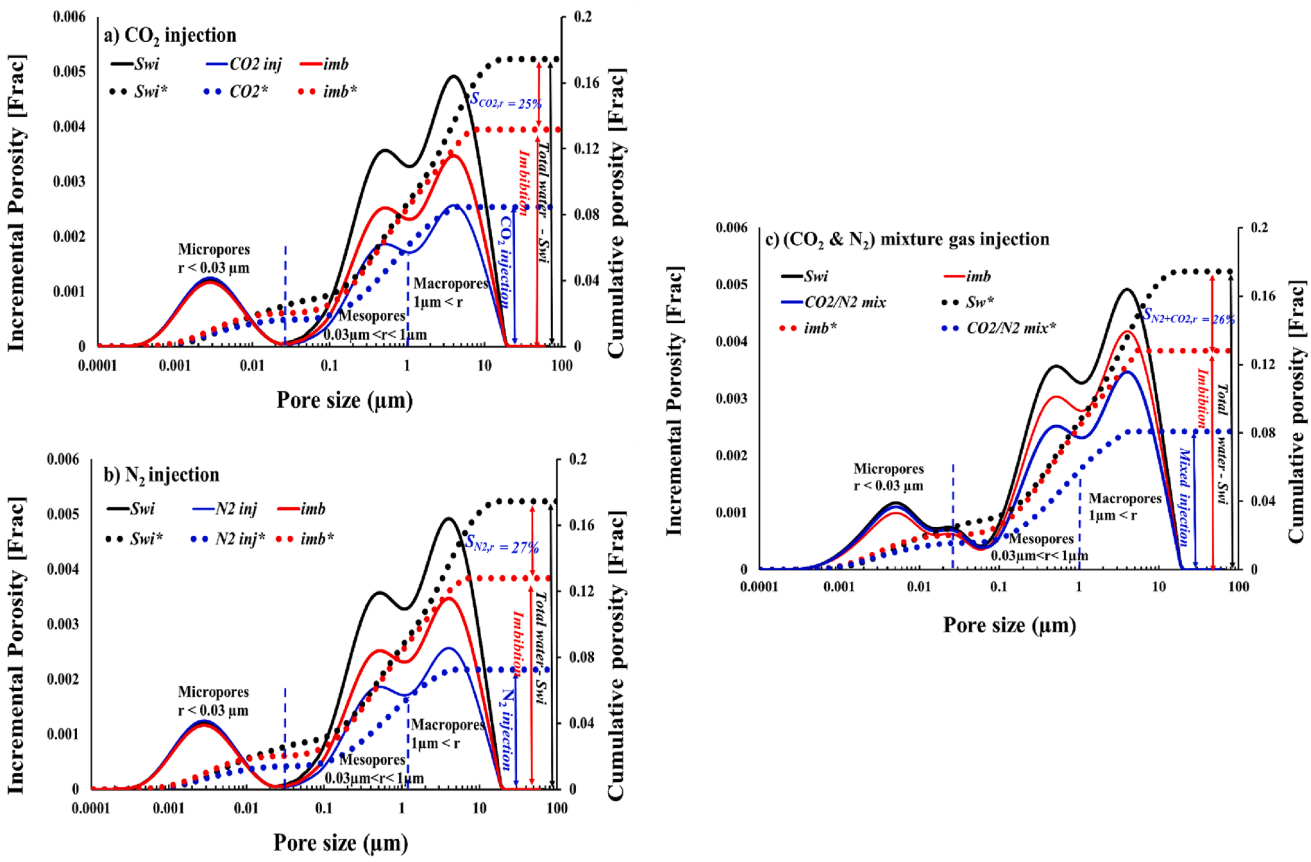

Fig. 6. The NMR profiles of water-wet Indiana limestone at 8 MPa and 333 K after secondary drainage and imbibition with each nonwetting gas: (a) $scCO_2$, (b) N_2, and (c) 50:50 CO_2-N_2. Here, the T_2 relaxation times were converted into pore radii by using Eq. (2). The solid curves represent the incremental volumes, while the dashed curves correspond to the cumulative volumes.

Table 4
The relationship between the relaxation time (T_2), pore type, and pore radius (r).

T_2 relaxation time (ms)	Pore type	Pore radius (r, µm)
≤ 3	micropores	$r \leq 0.03$
3–200	mesopores	$0.03 < r < 1$
200–2000	macropores	$1 < r$

intermediate pores. This is consistent with the literature and is typical of hydrophilic systems, where the relative position of each fluid in the pore system is controlled by the wettability and morphological properties of that system [102]. Mechanistically, the surface layer of water in the pore throat swells and eventually coalesces to fill the entire throat, while the nonwetting phase is left stranded in the form of large clusters (ganglia) in the pore space, thus resulting in disconnection and trapping (snap-off) of the nonwetting phase in the centers of the adjacent pores [18,103–106]. Subsequently, the water advances from the narrow throat to a broader site (i.e., a pore), thus leading to an abrupt saturation fluctuation and redistribution of the fluids in the pore space (Figs. 4 and 5).

4. Conclusions and implications

Carbon capture and sequestration (CCS) in geological formations is a prominent solution for effectively reducing the anthropogenic carbon emissions that mainly arise from the high consumption of fossil fuels. In this respect, the capillary trapping of CO_2 is a primary trapping mechanism that is governed by the pressure difference between the wetting and nonwetting phases in a porous rock, which makes the latter a key input parameter in dynamic simulation models. However, contamination of the CO_2 by impurities from various surface and subsurface sources can occur throughout the CCS operational process. Such contamination may highly impact the overall CO_2 wettability, storage capacity, and containment security. Hence, the present study used a robust gas-brine coreflooding system to acquire the nuclear magnetic resonance (NMR) longitudinal–transverse relaxation time (T_1-T_2) profiles, 2D maps, and absolute T_2 values in order to quantify the capillary trapping effect, wettability, and residual gas saturation of a water-wet Indiana limestone after cyclic secondary drainage/imbibition at 8 MPa and 333 K. To this end, three distinct gas-brine coreflood experiments were performed by using pure CO_2, pure N_2, and a 50:50 CO_2-N_2 mixture. Thus, when 10 pore volumes (PV) of supercritical CO_2 ($scCO_2$) were injected into the fully brine-saturated limestone sample, a significant amount of CO_2 was found to displace the brine and become trapped in the large (meso- and macro-scale) pores. The NMR T_2 relaxation time distributions indicated that the non-wetting phase (gas) displaced the wetting phase (water) from both the large pores ($r > 1$ µm) and the intermediate pores (0.03 µm $< r <$ 1 µm), while the water content of the small pores ($r <$ 0.03 µm) remained unchanged. Further, the residual saturations of CO_2, N_2, and 50:50 CO_2-N_2 after the 10 PV injections were 25%, 27%, 26%, respectively, with the coreflooding of 50:50 CO_2-N_2 providing an almost identical residual gas saturation to that of the CO_2-brine system. The negligible effect of the investigated impurity (N_2) in the mixed gas on the capillary trapping capacity clearly demonstrates that the presence of some impurities in the CO_2 for injection into carbonate formations during large-scale CCS projects can be tolerated without affecting the overall geo-storage containment effect. This has the potential benefit of substantial cost reduction due to the reduced amount of processing required for the removal of N_2 from the CO_2-rich flue gas.

In brief, the main findings of the present study were as follows:

- Allowing some impurities (such as N_2, O_2, or SOx) can be a financially feasible and cost-effective choice in the future planning and implementation of CCS schemes;
- The core flooding with CO_2 or mixed CO_2-N_2 gases lower the hydrophilic characteristics of Indiana limestone, which is detrimental to the geo-storage and containment security. Hence, further study is required in order to optimize the core-flooding process.

Thus, the present work provides fundamental insights into various implications of the geo-storage of CO_2 that should be considered in the large-scale implementation of CCS projects in geological formations.

Declaration of Competing Interest

The authors declare that they have no known competing financial interests or personal relationships that could have appeared to influence the work reported in this paper.

Data availability

No data was used for the research described in the article.

Acknowledgment

The authors would like to acknowledge King Abdullah University for Science and Technology (KAUST) and Edith Cowan University for providing the required infrastructure for this work.

References

[1] Bui M, Adjiman CS, Bardow A, Anthony EJ, Boston A, Brown S, et al. Carbon capture and storage (CCS): the way forward. Energy Environ Sci 2018;11(5):1062–176.
[2] Datta A, De Leon R, Krishnamoorti R. Advancing carbon management through the global commoditization of CO2: the case for dual-use LNG-CO2 shipping. Carbon Manag 2020;11(6):611–30.
[3] Hordeski MF. Megatrends for Energy Efficiency and Renewable Energy 2020. https://doi.org/10.1201/9781003151616.
[4] Pacala S, Socolow R. Stabilization wedges: Solving the climate problem for the next 50 years with current technologies. Science (80-) 2004;305:968–72. doi: 10.1126/SCIENCE.1100103/SUPPL_FILE/PACALA.SOM.PDF.
[5] Ali M, Jha NK, Pal N, Keshavarz A, Hoteit H, Sarmadivaleh M. Recent advances in carbon dioxide geological storage, experimental procedures, influencing parameters, and future outlook. Earth-Science Rev 2022:225. https://doi.org/10.1016/J.EARSCIREV.2021.103895.
[6] Masson-Delmotte V, Zhai P, Pörtner H-O, Roberts D, Skea J, Shukla PR, et al. Summary for Policymakers. Global Warming of 1.5°C. An IPCC Special Report on the impacts of global warming of 1.5 °C above pre-industrial levels. 2018.
[7] Treut L, Somerville R, Cubasch U, Ding Y, Mauritzen C, Mokssit a, et al. Historical Overview of Climate Change Science. Earth 2007;Chapter 1. doi: 10.1016/j.soilbio.2010.04.001.
[8] Shukla R, Ranjith P, Haque A, Choi X. A review of studies on CO2 sequestration and caprock integrity. Fuel 2010;89(10):2651–64.
[9] Cranganu C, Soleymani H. Carbon dioxide sealing capacity: Textural or compositional controls? A case study from the Oklahoma Panhandle. Environ Geosci 2015;22(2):57–74.
[10] Bartlett EP, Hetherington HC, Kvalnes HM, Tremearne TH. THE COMPRESSIBILITY ISOTHERMS OF HYDROGEN, NITROGEN AND A 3:1 MIXTURE OF THESE GASES AT TEMPERATURES OF -70, -50, -25 AND 20° AND AT PRESSURES TO 1000 ATMOSPHERES. J Am Chem Soc 2002;52:1363–73. doi: 10.1021/JA01367A011.
[11] Orr FM. Onshore geologic storage of CO2. Science (80-) 2009;325:1656–8. doi: 10.1126/SCIENCE.1175677/ASSET/CB2F0D94-0559-431E-A069-0894080091BF/ASSETS/GRAPHIC/325_1656_F1.JPEG.
[12] Raza A, Gholami R, Rezaee R, Rasouli V, Rabiei M. Significant aspects of carbon capture and storage – A review. Petroleum 2019;5(4):335–40.
[13] Zhang D, Song J. Mechanisms for geological carbon sequestration. Procedia IUTAM 2014;10:319–27.
[14] Ajayi T, Gomes JS, Bera A. A review of CO2 storage in geological formations emphasizing modeling, monitoring and capacity estimation approaches. Pet Sci 2019;16(5):1028–63.
[15] Aminu MD, Nabavi SA, Rochelle CA, Manovic V. A review of developments in carbon dioxide storage. Appl Energy 2017;208:1389–419.
[16] Kumar A, Ozah R, Noh M, Pope GA, Bryant S, Sepehmoori K, et al. Reservoir simulation of CO2 storage in deep saline aquifers. SPE J 2005;10:336–48. https://doi.org/10.2118/89343-pa.
[17] Iglauer S, Pentland CH, Busch A. CO2 wettability of seal and reservoir rocks and the implications for carbon geo-sequestration. Water Resour Res 2015;51:729–74. https://doi.org/10.1002/2014WR015553.
[18] Baban A, Keshavarz A, Amin R, Iglauer S. Residual Trapping of CO2 and Enhanced Oil Recovery in Oil-Wet Sandstone Core – A Three-Phase Pore-Scale Analysis Using NMR. Fuel 2023:332. https://doi.org/10.1016/J.FUEL.2022.126000.
[19] Baban A, Keshavarz A, Amin R, Iglauer S. Impact of Wettability Alteration on CO 2 Residual Trapping in Oil-Wet Sandstone at Reservoir Conditions Using Nuclear Magnetic Resonance. Energy Fuel 2022;36(22):13722–31.
[20] Blunt MJ. Multiphase Flow in Permeable Media. n.d. doi: 10.1017/9781316145098.
[21] Ali M, Aftab A, Arain Z-U-A, Al-Yaseri A, Roshan H, Saeedi A, et al. Influence of Organic Acid Concentration on Wettability Alteration of Cap-Rock: Implications for CO2Trapping/Storage. ACS Appl Mater Interfaces 2020;12(35):39850–8.
[22] Al-Khdheeawi EA, Mahdi DS, Ali M, Fauziah CA, Barifcani A. Impact of Caprock Type on Geochemical Reactivity and Mineral Trapping Efficiency of CO2. Offshore Technol Conf Asia 2020, OTCA 2020 2020. doi: 10.4043/30094-MS.
[23] Rahman T, Lebedev M, Barifcani A, Iglauer S. Residual trapping of supercritical CO2 in oil-wet sandstone. J Colloid Interface Sci 2016;469:63–8.
[24] Chaudhary K, Bayani Cardenas M, Wolfe WW, Maisano JA, Ketcham RA, Bennett PC. Pore-scale trapping of supercritical CO2 and the role of grain wettability and shape. Geophys Res Lett 2013;40(15):3878–82.
[25] Al-Menhali AS, Menke HP, Blunt MJ, Krevor SC. Pore Scale Observations of Trapped CO2 in Mixed-Wet Carbonate Rock: Applications to Storage in Oil Fields. Environ Sci Technol 2016;50(18):10282–90.
[26] Iglauer S. CO2-Water-Rock Wettability: Variability, Influencing Factors, and Implications for CO2 Geostorage. Acc Chem Res 2017;50(5):1134–42.
[27] Sun Y, Li Qi, Yang D, Liu X. Laboratory core flooding experimental systems for CO2 geosequestration: An updated review over the past decade. J Rock Mech Geotech Eng 2016;8(1):113–26.
[28] Levine JS, Goldberg DS, Lackner KS, Matter JM, Supp MG, Ramakrishnan TS. Relative permeability experiments of carbon dioxide displacing brine and their implications for carbon sequestration. Environ Sci Technol 2014;48(1):811–8.
[29] Nguyen P, Fadaei H, Sinton D. Microfluidics underground: A micro-core method for pore scale analysis of supercritical CO2 reactive transport in saline aquifers. J Fluids Eng Trans ASME 2013:135. https://doi.org/10.1115/1.4023644.
[30] Sharbatian A, Abedini A, Qi Z, Sinton D. Full Characterization of CO2-Oil Properties On-Chip: Solubility, Diffusivity, Extraction Pressure, Miscibility, and Contact Angle. Anal Chem 2018;90:2461–7. https://doi.org/10.1021/ACS.ANALCHEM.7B05358/SUPPL_FILE/AC7B05358_SI_001.PDF.
[31] Seo S, Mastiani M, Hafez M, Kunkel G, Ghattas Asfour C, Garcia-Ocampo KI, et al. Injection of in-situ generated CO2 microbubbles into deep saline aquifers for enhanced carbon sequestration. Int J Greenh Gas. Control 2019;83:256–64.
[32] Abolhasani M, Günther A, Kumacheva E. Microfluidic studies of carbon dioxide. Angew Chemie - Int Ed 2014;53(31):7992–8002.
[33] Saraf S, Bera A. A review on pore-scale modeling and CT scan technique to characterize the trapped carbon dioxide in impermeable reservoir rocks during sequestration. Renew Sustain Energy Rev 2021:144. https://doi.org/10.1016/j.rser.2021.110986.
[34] Jiang F, Tsuji T. Estimation of three-phase relative permeability by simulating fluid dynamics directly on rock-microstructure images. Water Resour Res 2017;53(1):11–32.
[35] Callow B, Falcon-Suarez I, Ahmed S, Matter J. Assessing the carbon sequestration potential of basalt using X-ray micro-CT and rock mechanics. Int J Greenh Gas. Control 2018;70:146–56.
[36] Ali M, Arif M, Sahito MF, Al-Anssari S, Keshavarz A, Barifcani A, et al. CO2-wettability of sandstones exposed to traces of organic acids: Implications for CO2 geo-storage. Int J Greenh Gas. Control 2019;83:61–8.
[37] Arif M, Barifcani A, Lebedev M, Iglauer S. Structural trapping capacity of oil-wet caprock as a function of pressure, temperature and salinity. Int J Greenh Gas Control 2016;50:112–20. https://doi.org/10.1016/J.IJGGC.2016.04.024.
[38] Chabab S, Théveneau P, Corvisier J, Coquelet C, Paricaud P, Houriez C, et al. Thermodynamic study of the CO2 – H2O – NaCl system: Measurements of CO2 solubility and modeling of phase equilibria using Soreide and Whitson, electrolyte CPA and SIT models. Int J Greenh Gas. Control 2019;91:102825.
[39] Alanazi A, Ali M, Bawazeer S, Yekeen N, Hoteit H. Evaluation of cubic, PC-SAFT, and GERG2008 equations of state for accurate calculations of thermophysical properties of hydrogen-blend mixtures. Energy Rep 2022;8:13876–99. https://doi.org/10.1016/J.EGYR.2022.10.257.
[40] Ibrahim AF, Abdelgawad KZ, Al-Anazi A, Al Hamad JS. Effect of Crude Oil Properties on the Interfacial Tension of Crude Oil/CO2 Under HPHT Conditions. Arab J Sci Eng 2023;48(7):9269–86.
[41] Ali M, Pan B, Yekeen N, Al-Anssari S, Al-Anazi A, Keshavarz A, et al. Assessment of wettability and rock-fluid interfacial tension of caprock: Implications for hydrogen and carbon dioxide geo-storage. Int J Hydrogen Energy 2022;47(30):14104–20.
[42] Messabeb H, Contamine F, Cézac P, Serin JP, Gaucher EC. Experimental Measurement of CO2 Solubility in Aqueous NaCl Solution at Temperature from 323.15 to 423.15 K and Pressure of up to 20 MPa. J Chem Eng Data 2016;61:3573–84. https://doi.org/10.1021/ACS.JCED.6B00505.

[43] Alanazi A, Bawazeer S, Ali M, Keshavarz A, Hoteit H. Thermodynamic Modeling of Hydrogen-Water Systems with Gas Impurity at Various Conditions Using Cubic and PC-SAFT Equations of State. Energy Convers Manag X 2022;15:100257.
[44] Wang J, Wang Z, Ryan D, Lan C. A study of the effect of impurities on CO2 storage capacity in geological formations. Int J Greenh Gas Control 2015;42:132–7. https://doi.org/10.1016/J.IJGGC.2015.08.002.
[45] Wang J, Ryan D, Anthony EJ, Wildgust N, Aiken T. Effects of impurities on CO2 transport, injection and storage. Energy Procedia 2011;4:3071–8.
[46] Marston PM, Moore P a. From EOR to CCS: The evolving legal and regulatory framework for carbon capture and storage. Energy Law J 2008;29.
[47] Jian Z, Yuanyuan Z, Yu Z, Qingfang Li, Haili L, Yinjun Lu, et al. Improvement of environmental monitoring technology on the basis of carbon mass balance during CO2-enhanced Oil recovery and storage. Energy Procedia 2014;63:3293–7.
[48] Bachu S. CO2 storage in geological media: Role, means, status and barriers to deployment. Prog Energy Combust Sci 2008;34(2):254–73.
[49] Haines M, Leslie J, Macdonald D. Co-capture and storage of CO2 with other impurities from coal and heavy fuel-fired power plant flue gases. Greenh Gas Control Technol 2005. https://doi.org/10.1016/B978-008044704-9/50030-6.
[50] Ziabakhsh-Ganji Z, Kooi H. Sensitivity of the CO2 storage capacity of underground geological structures to the presence of SO2 and other impurities. Appl Energy 2014;135:43–52.
[51] Miri R, Aagaard P, Hellevang H. Examination of CO2-SO2 solubility in water by SAFT1. Implications for CO2 transport and storage. J Phys Chem B 2014;118(34):10214–23.
[52] Moysan JM, Paradowski H, Vidal J. Prediction of phase behaviour of gas-containing systems with cubic equations of state. Chem Eng Sci 1986;41(8):2069–74.
[53] Shar AM, Ali M, Bhutto DK, Alanazi A, Akhondzadeh H, Keshavarz A, et al. Cryogenic Liquid Nitrogen Fracking Effects on Petro-Physical and Morphological Characteristics of the Sembar Shale Gas Formation in the Lower Indus Basin. Pakistan Energy & Fuels 2022. https://doi.org/10.1021/ACS.ENERGYFUELS.2C02257/ASSET/IMAGES/LARGE/EF2C02257_0008.JPEG.
[54] Alanazi A, Al Malallah M, Mowafi M, Badeghaish W, Hoteit H, Al-Yaseri A, et al. Hydrogen Wettability Measurement of Saudi Basaltic Rocks at Underground Storage Conditions. All Days 2022. https://doi.org/10.56952/IGS-2022-110.
[55] Baban A, Hosseini M, Keshavarz A, Amin R, Ali M, Iglauer S. Residual Co2 Trapping and Enhanced Oil Recovery in Carbonate Reservoirs: Three-Phase Flow Dynamics Examined Via Nmr. SSRN Electron J 2022. https://doi.org/10.2139/SSRN.4313240.
[56] Churchel PL, French PB, Shaw JC, Schramm LL. Rock properties of Berea sandstone, Baker dolomite, and Indiana limestone, 1991. doi: 10.2523/21044-ms.
[57] Micon J. Limestone prophets: Gauging the effectiveness of religious political action organizations that lobby state legislatures. Sociol Relig A Q Rev 2008;69(4):397–413.
[58] El-Maghraby RM, Blunt MJ. Residual CO2 trapping in Indiana limestone. Environ Sci Technol 2013;47(1):227–33.
[59] Baban A, Al-Yaseri A, Keshavarz A, Amin R, Iglauer S. CO2 – brine – sandstone wettability evaluation at reservoir conditions via Nuclear Magnetic Resonance measurements. Int J Greenh Gas Control 2021;111:103435. https://doi.org/10.1016/J.IJGGC.2021.103435.
[60] Al-Yaseri A, Esteban L, Giwelli A, Sarout J, Lebedev M, Sarmadivaleh M. Initial and residual trapping of hydrogen and nitrogen in Fontainebleau sandstone using nuclear magnetic resonance core flooding. Int J Hydrogen Energy 2022;47:22482–94. https://doi.org/10.1016/J.IJHYDENE.2022.05.059.
[61] Ali M, Al-Yaseri A, Awan FUR, Arif M, Keshavarz A, Iglauer S. Effect of water-soluble organic acids on wettability of sandstone formations using streaming zeta potential and NMR techniques: Implications for CO2 geo-sequestration. Fuel 2022;329:125449. https://doi.org/10.1016/J.FUEL.2022.125449.
[62] Span R, Wagner W. A new equation of state for carbon dioxide covering the fluid region from the triple-point temperature to 1100 K at pressures up to 800 MPa. J Phys Chem Ref Data 1996;25. doi: 10.1063/1.555991.
[63] Iglauer S, Lebedev M. High pressure-elevated temperature x-ray micro-computed tomography for subsurface applications. Adv Colloid Interface Sci 2018;256:393–410.
[64] Ali M, Sahito MF, Jha NK, Arain Z-U-A, Memon S, Keshavarz A, et al. Effect of nanofluid on CO2-wettability reversal of sandstone formation; implications for CO2 geo-storage. J Colloid Interface Sci 2020;559:304–12.
[65] Mohamed IM, He J, Nasr-El-Din HA. Carbon dioxide sequestration in dolomite rock. Soc. Pet. Eng. - Int. Pet. Technol. Conf. 2012, IPTC 2012, vol. 3, 2012.
[66] Nhunduru RAE, Jahanbakhsh A, Shahrokhi O, Wlodarczyk KL, Garcia S, Maroto-Valer MM. The Impact of Wettability on Dynamic Fluid Connectivity and Flow Transport Kinetics in Porous Media. Water Resour Res 2022;58:e2021WR030729. doi: 10.1029/2021WR030729.
[67] Mohanty KK. Porous media: Fluid transport and pore structure. By F. A. L. Dullien, Academic Press, 574 pp., 1992. AIChE J 1992;38(8):1303–4.
[68] Iglauer S, Paluszny A, Pentland CH, Blunt MJ. Residual CO2 imaged with X-ray micro-tomography. Geophys Res Lett 2011;38:1–6. https://doi.org/10.1029/2011GL049680.
[69] Almenningen S, Roy S, Hussain A, Seland JG, Ersland G. Effect of mineral composition on transverse relaxation time distributions and mr imaging of tight rocks from offshore Ireland. Minerals 2020:10. https://doi.org/10.3390/min10030232.
[70] McCaffery FG, Bennion DW. The Effect OfWettability On Two-Phase Relative Penneabilities. J Can Pet Technol 1974:13. https://doi.org/10.2118/74-04-04.
[71] Valori A, Nicot B. A review of 60 years of nmr wettability. Petrophysics 2019;60(2):255–63.
[72] Katika K, Saidian M, Prasad M, Fabricius IL. Low-field NMR spectrometry of chalk and argillaceous sandstones: Rock-fluid affinity assessed from T1/T2 ratio. Petrophysics 2017;58.
[73] Valori A, Hursan G, Ma SM. Laboratory and Downhole Wettability from NMR T1/T2 Ratio. Petrophysics 2017;58.
[74] Coates GR, Xiao L, Prammer MG. NMR logging. Ebooks; 1999.
[75] Wang X, Alvarado V, Swoboda-Colberg N, Kaszuba JP. Reactivity of dolomite in water-saturated supercritical carbon dioxide: Significance for carbon capture and storage and for enhanced oil and gas recovery. Energy Convers Manag 2013;65:564–73.
[76] Korb JP. Nuclear magnetic relaxation of liquids in porous media. New J Phys 2011:13. https://doi.org/10.1088/1367-2630/13/3/035016.
[77] Washburn KE, Sandor M, Cheng Y. Evaluation of sandstone surface relaxivity using laser-induced breakdown spectroscopy. J Magn Reson 2017;275:80–9.
[78] Li M, Vogt SJ, May EF, Johns ML. In Situ CH4–CO2 Dispersion Measurements in Rock Cores. Transp Porous Media 2019;129(1):75–92.
[79] Khatibi S, Ostadhassan M, Xie ZH, Gentzis T, Bubach B, Gan Z, et al. NMR relaxometry a new approach to detect geochemical properties of organic matter in tight shales. Fuel 2019;235:167–77.
[80] Abramov A, Keshavarz A, Iglauer S. Wettability of Fully Hydroxylated and Alkylated (001) α-Quartz Surface in Carbon Dioxide Atmosphere. J Phys Chem C 2019;123:9027–40. https://doi.org/10.1021/ACS.JPCC.9B00263/SUPPL_FILE/JP9B00263_SI_001.PDF.
[81] AlRatrout A, Blunt MJ, Bijeljic B. Wettability in complex porous materials, the mixed-wet state, and its relationship to surface roughness. Proc Natl Acad Sci U S A 2018;115(36):8901–6.
[82] Linstrom PJ, Mallard WG. The NIST Chemistry WebBook: A chemical data resource on the Internet. J Chem Eng Data 2001;46:1059–63. https://doi.org/10.1021/je000236i.
[83] Arif M, Lebedev M, Barifcani A, Iglauer S. Influence of shale-total organic content on CO2 geo-storage potential. Geophys Res Lett 2017;44:8769–75. https://doi.org/10.1002/2017GL073532.
[84] Berg S, Oedai S, Ott H. Displacement and mass transfer between saturated and unsaturated CO2-brine systems in sandstone. Int J Greenh Gas. Control 2013;12:478–92.
[85] Al-Yaseri AZ, Lebedev M, Barifcani A, Iglauer S. Receding and advancing (CO2 + brine + quartz) contact angles as a function of pressure, temperature, surface roughness, salt type and salinity. J Chem Thermodyn 2016;93:416–23. https://doi.org/10.1016/J.JCT.2015.07.031.
[86] Adamczyk K, Prémont-Schwarz M, Pines D, Pines E, Nibbering and ETJ. Real-Time Observation of Carbonic. 2009.
[87] Korb JP, Freiman G, Nicot B, Ligneul P. Dynamical surface affinity of diphasic liquids as a probe of wettability of multimodal porous media. Phys Rev E - Stat Nonlinear, Soft Matter Phys 2009;80:061601. https://doi.org/10.1103/PHYSREVE.80.061601/FIGURES/7/MEDIUM.
[88] Valvatne PH, Blunt MJ. Predictive pore-scale modeling of two-phase flow in mixed wet media. Water Resour Res 2004;40:1–21. https://doi.org/10.1029/2003WR002627.
[89] Alhosani A, Scanziani A, Lin Q, Foroughi S, Alhammadi AM, Blunt MJ, et al. Dynamics of water injection in an oil-wet reservoir rock at subsurface conditions: Invasion patterns and pore-filling events. Phys Rev E 2020;102:23110. https://doi.org/10.1103/PhysRevE.102.023110.
[90] Lebedev M, Zhang Y, Sarmadivaleh M, Barifcani A, Al-Khdheeawi E, Iglauer S. Carbon geosequestration in limestone: Pore-scale dissolution and geomechanical weakening. Int J Greenh Gas Control 2017;66. doi: 10.1016/j.ijggc.2017.09.016.
[91] Gharbi O, Bijeljic B, Boek E, Blunt MJ. Changes in pore structure and connectivity induced by CO2 injection in carbonates: A combined pore-scale approach. Energy Procedia 2013;37:5367–78. https://doi.org/10.1016/j.egypro.2013.06.455.
[92] Luquot L, Rodriguez O, Gouze P. Experimental Characterization of Porosity Structure and Transport Property Changes in Limestone Undergoing Different Dissolution Regimes. Transp Porous Media 2014;101:507–32. https://doi.org/10.1007/s11242-013-0257-4.
[93] Adamson. Physical Chemistry of Surfaces. 1960.
[94] Wang Y, Bedrikovetsky P, Yin H, Othman F, Zeinijahromi A, Le-Hussain F. Analytical model for fines migration due to mineral dissolution during CO2 injection. J Nat Gas Sci Eng 2022:100. https://doi.org/10.1016/j.jngse.2022.104472.
[95] Iglauer S. Dissolution Trapping of Carbon Dioxide in Reservoir Formation Brine – A Carbon Storage Mechanism. Mass Transf - Adv Asp 2011. https://doi.org/10.5772/20206.
[96] Cai Y, Chen H, Liu P, Chen J, Xu H, Alshahrani T, et al. Robust microporous hydrogen−bonded organic framework for highly selective purification of methane from natural gas. Microporous Mesoporous Mater 2023;352:112495.
[97] Al-Menhali AS, Krevor S. Capillary Trapping of CO2 in Oil Reservoirs: Observations in a Mixed-Wet Carbonate Rock. Environ Sci Technol 2016;50(5):2727–34.
[98] Zhang Y, Sarmadivaleh M, Lebedev M, Barifcani A, Rezaee R, Testamantia N, et al. Geo-mechanical weakening of limestone due to supercritical CO2 injection. Offshore Technol Conf Asia 2016, OTCA 2016 2016;4:1966–73. doi: 10.4043/26470-ms.
[99] Vialle S, Contraires S, Zinzsner B, Clavaud J-B, Mahiouz K, Zuddas P, et al. Percolation of CO2-rich fluids in a limestone sample: Evolution of hydraulic, electrical, chemical, and structural properties. J Geophys Res Solid Earth 2014;119(4):2828–47.
[100] Wang S, Tokunaga TK. Capillary Pressure-Saturation Relations for Supercritical CO2 and Brine in Limestone/Dolomite Sands: Implications for Geologic Carbon

Sequestration in Carbonate Reservoirs. Environ Sci Technol 2015;49:7208–17. https://doi.org/10.1021/acs.est.5b00826.

[101] Mangane PO, Gouze P, Luquot L. Permeability impairment of a limestone reservoir triggered by heterogeneous dissolution and particles migration during CO2-rich injection. Geophys Res Lett 2013;40:4614–9. https://doi.org/10.1002/grl.50595.

[102] Zulfiqar B, Vogel H, Ding Y, Golmohammadi S, Küchler M, Reuter D, et al. The Impact of Wettability and Surface Roughness on Fluid Displacement and Capillary Trapping in 2-D and 3-D Porous Media: 2. Combined Effect of Wettability, Surface Roughness, and Pore Space Structure on Trapping Efficiency in Sand Packs and Micromodels. Water Resour Res 2020;56. doi: 10.1029/2020WR027965.

[103] ROOF JG. SNAP-OFF OF OIL DROPLETS IN WATER- WET PORES. Soc Pet Eng J 1970;10. doi: 10.2118/2504-pa.

[104] Bachu S, Adams JJ. Sequestration of CO2 in geological media in response to climate change: Capacity of deep saline aquifers to sequester CO2 in solution. Energy Convers Manag 2003;44(20):3151–75.

[105] Bakhshian S, Rabbani HS, Shokri N. Physics-Driven Investigation of Wettability Effects on Two-Phase Flow in Natural Porous Media: Recent Advances, New Insights, and Future Perspectives. Transp Porous Media 2021;140(1):85–106.

[106] Broseta D, Tonnet N, Shah V. Are rocks still water-wet in the presence of dense CO2 or H2S? Geofluids 2012;12:280–94. https://doi.org/10.1111/J.1468-8123.2012.00369.X.